

# Proline-based allosteric inhibitors of Zika and Dengue virus NS2B/NS3 proteases

*Benedikt Millies,<sup>†</sup> Franziska von Hammerstein,<sup>†</sup> Andrea Gellert,<sup>†</sup> Stefan Hammerschmidt,<sup>†</sup> Fabian Barthels,<sup>†</sup> Ulrike Göppel,<sup>†</sup> Melissa Immerheiser,<sup>⊥</sup> Fabian Elgner,<sup>||</sup> Nathalie Jung<sup>⊥</sup>, Michael Basic,<sup>||</sup> Christian Kersten,<sup>†</sup> Werner Kiefer,<sup>†</sup> Jochen Bodem,<sup>⊥</sup> Eberhard Hildt,<sup>||</sup> Maïke Windbergs<sup>⊥</sup>, Ute A. Hellmich,<sup>‡,§,#</sup> Tanja Schirmeister<sup>‡,#</sup>*

<sup>†</sup>Institute of Pharmacy and Biochemistry, Johannes Gutenberg University Mainz, Staudinger Weg 5,  
55128 Mainz, Germany

<sup>⊥</sup>Institut für Virology und Immunbiologie, Julius-Maximilians-Universität Würzburg, Versbacher Str. 7,  
97078 Würzburg, Germany

<sup>||</sup>Department of Virology, Paul-Ehrlich-Institut, 63225 Langen, Germany

<sup>‡</sup>Institute of Pharmacy and Biochemistry, Johannes Gutenberg University Mainz, Johann-Joachim-  
Becherweg 30, 55128 Mainz, Germany

<sup>§</sup>Center for Biomolecular Magnetic Resonance (BMRZ), Goethe-Universität, 60438 Frankfurt am Main,  
Germany

<sup>⊥</sup> Institute of Pharmaceutical Technology and Buchmann Institute for Molecular Life Sciences, Goethe  
University, Max-von-Laue-Straße 15, 60438 Frankfurt am Main, Germany

## Table of Contents

<b>1</b>	<b>Determination of enantiomeric ratios</b>	<b>3</b>
<b>2</b>	<b>IC<sub>50</sub> Determinations at different substrate concentrations</b>	<b>4</b>
<b>3</b>	<b>Hydrophilicity determination of synthesized compounds</b>	<b>4</b>
<b>4</b>	<b>CD Spectroscopy studies of cysteine mutants</b>	<b>7</b>
<b>5</b>	<b>Docking Studies</b>	<b>11</b>
<b>6</b>	<b>MD</b>	<b>17</b>
<b>7</b>	<b>Antiviral activity</b>	<b>21</b>
<b>8</b>	<b>Cell permeability</b>	<b>28</b>
<b>9</b>	<b>Overview of all manuscript compounds with numbers</b>	<b>29</b>
<b>10</b>	<b>References</b>	<b>41</b>

# 1 DETERMINATION OF ENANTIOMERIC RATIOS

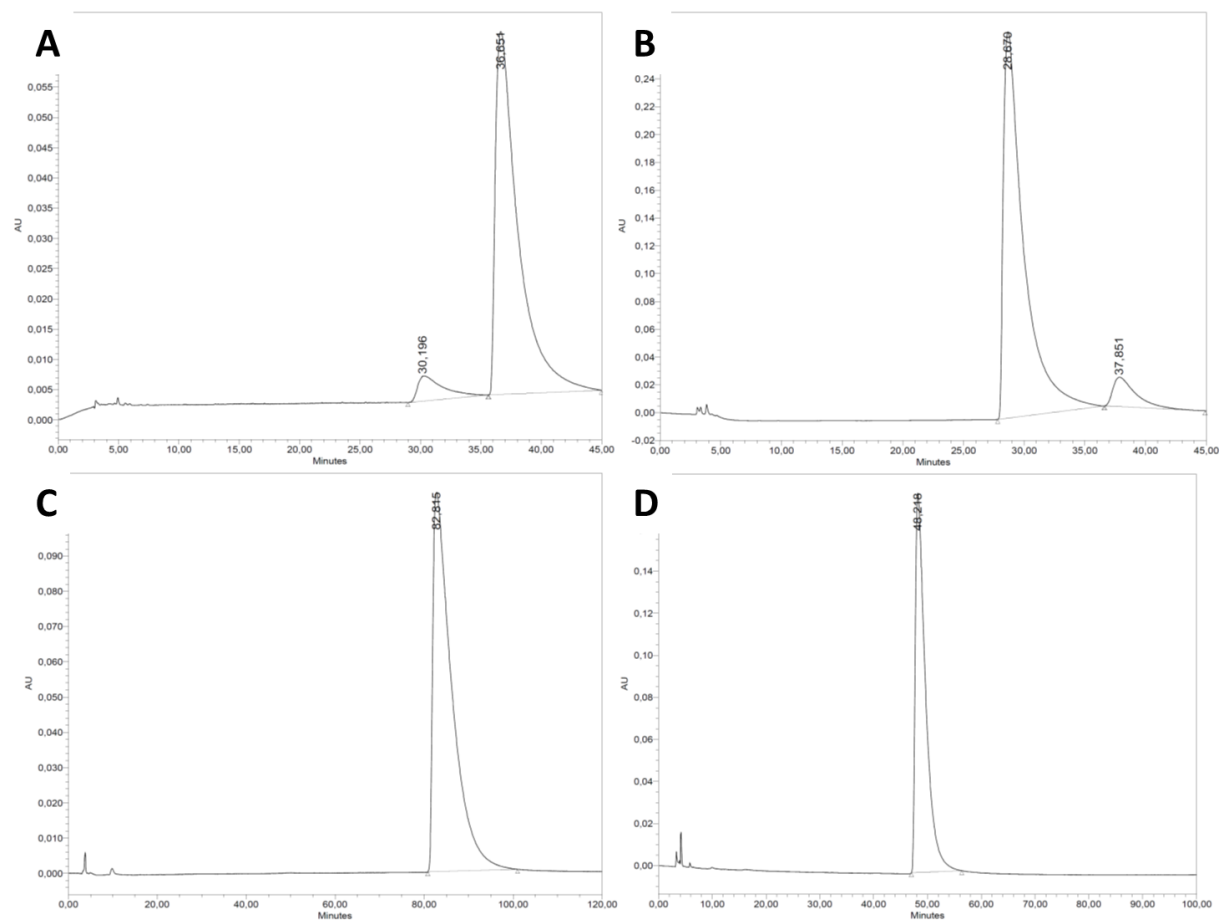


**Figure SI1.** Chromatograms for the determination of enantiomeric ratios of (*R*)-**7** (A), (*S*)-**7** (B), (*R*)-**18** (C) and (*S*)-**18** (D) by HPLC at 254 nm.

## 2 IC<sub>50</sub> DETERMINATIONS AT DIFFERENT SUBSTRATE CONCENTRATIONS

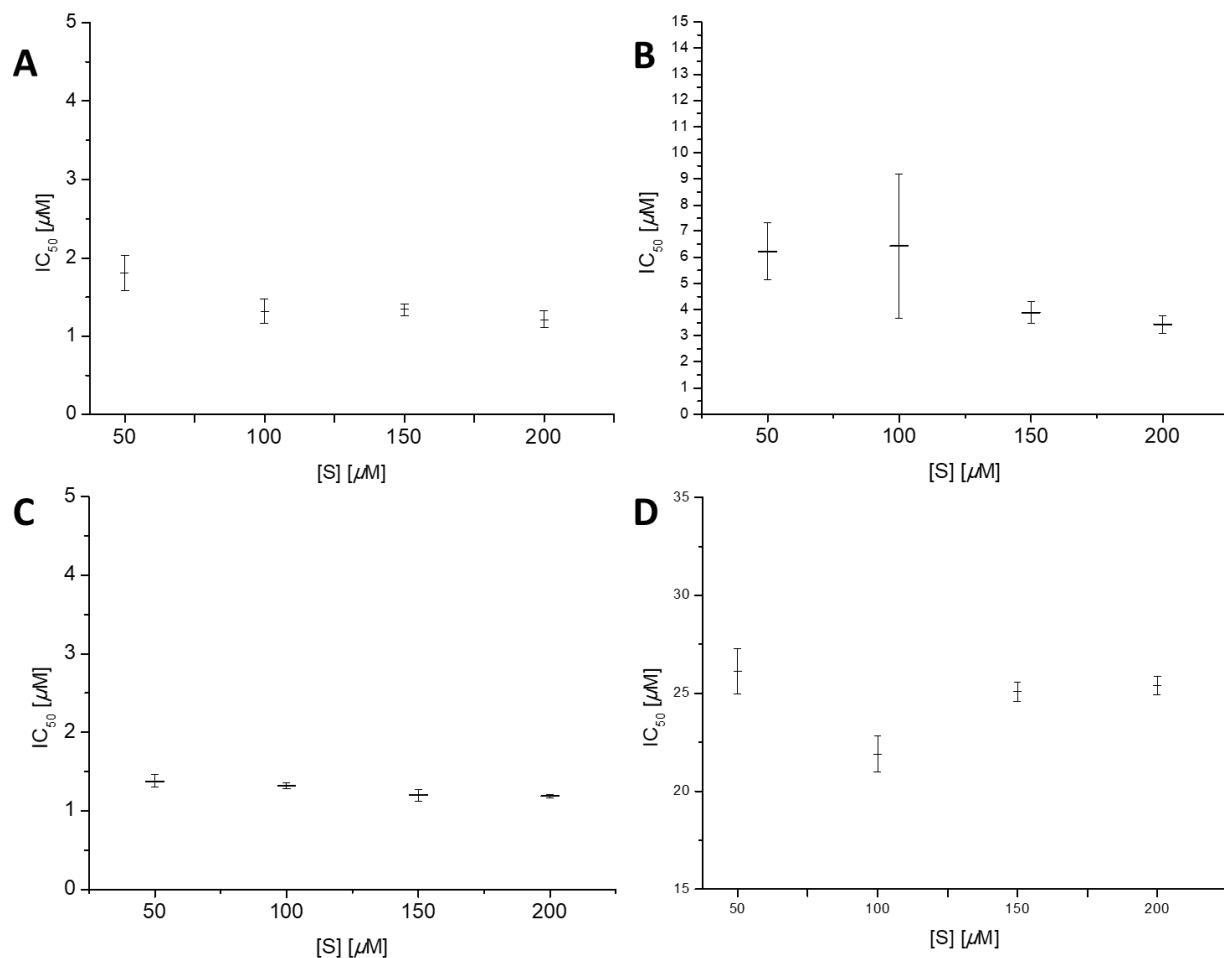


**Figure SI 2.** IC<sub>50</sub> values of inhibitors **1** (A), **35** (B), (*R*)-**7** (C) and (*R*)-**21** (D) measured on the ZIKV NS2B/NS3 protease at different substrate concentrations. IC<sub>50</sub> values are indicated as means  $\pm$  standard deviation from three independent measurements each, performed in duplicates.

## 3 HYDROPHILICITY DETERMINATION OF SYNTHESIZED COMPOUNDS

SlogP values were calculated with Moe, version 2015.1001, with the SlogP descriptor.<sup>1</sup> Retention times were collected on the LC-MS system described in the experimental section. The lipophilic ligand efficiencies LLE were calculated using the following equation:

$$LLE = pK_i - clogP$$

**Table SI1.** SlogP values, retention times and lipophilicity ligand efficiencies (LLE) of the synthesized compounds.

Compound	SlogP	t <sub>R</sub>	LLE
<b>1</b>	5.61	1.98	0.24
<b>6a</b>	2.95	0.78	3.08
<b>6b</b>	2.95	0.78	2.86
<b>7a</b>	2.81	1.26	3.07
<b>7b</b>	2.81	1.30	3.07
<b>8a</b>	2.50	1.03	3.23
<b>8b</b>	2.50	1.01	3.35
<b>9</b>	2.64	1.16	3.35
<b>10a</b>	3.15	1.54	2.70
<b>10b</b>	3.15	1.57	2.88
<b>11a</b>	2.51	1.11	3.56
<b>11b</b>	2.51	1.09	3.37
<b>12a</b>	2.41	1.16	4.09
<b>12b</b>	2.41	1.18	3.62
<b>13a</b>	4.17	2.84	1.44
<b>13b</b>	4.17	2.93	1.33
<b>14a</b>	2.41	1.12	3.55
<b>14b</b>	2.41	1.11	3.34
<b>15a</b>	3.61	0.82	2.26
<b>15b</b>	3.61	0.83	1.92
<b>26</b>	3.06	1.38	2.29
<b>30a</b>	3.20	1.79	3.04
<b>30b</b>	3.20	1.82	3.09

<b>31</b>	2.72	0.80	3.37
<b>32</b>	3.06	1.33	2.17
<b>35</b>	4.07	2.15	1.12

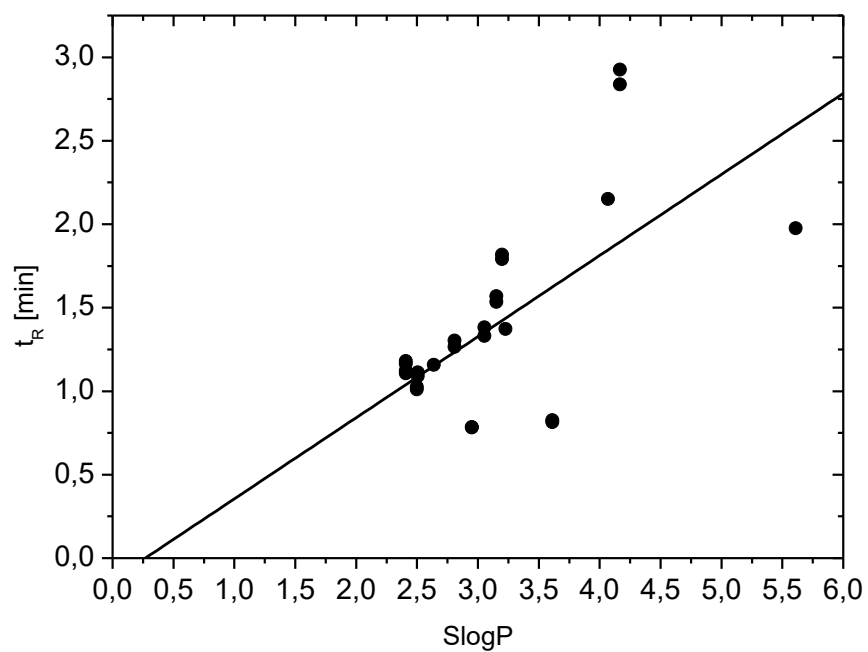


**Figure SI3.** Correlation of calculated SlogP values with retention times from RP-HPLC runs.

Shown is the regression line.

#### 4 CD SPECTROSCOPY STUDIES OF CYSTEINE MUTANTS

**MATERIALS AND METHODS** Samples of maleimide (MI) -coupled proteases were prepared by diluting 20 mM stock solutions of BMI and EMI with H<sub>2</sub>O to a concentration of 200  $\mu$ M. To 81  $\mu$ M stock solutions of DENV2 A164C and A166C mutants, a twofold excess of either BMI or EMI was added and the mixture was incubated for coupling over 10 minutes at room temperature and afterwards diluted with H<sub>2</sub>O and gel filtration buffer to 5  $\mu$ M protein concentration, Tris HCl 1.25 mM and NaCl 10 mM.

All CD spectra were measured at room temperature using a JASCO J.815 CD-spectrometer. Control references were carried out with identically treated buffer of the same composition.

The far-UV measurements were conducted 3 times each in the 260 – 190 nm spectral range using a scanning speed of 50 nm min<sup>-1</sup>, a 5 nm spectral bandwidth, 0.5 s data integration time, a 1 nm data pitch and an accumulation cycle of 5. Spectra were processed with the Jasco Spectra Analysis software (Tokyo, Japan) and analyzed using the Beta Structure Selection method (BeStSel).

**RESULTS AND DISCUSSIONS** The voltage occurring while performing CD measurements at low wavelengths is a limiting factor of obtaining accurate spectra.<sup>2</sup> Therefore, the salt buffer and DMSO concentrations should be kept constant and as low as tolerated by the measured protein.

Diluting the maleimide (MI) to 200  $\mu$ M with DMSO prior to reaction with the protease and subsequent CD measurements resulted in a voltage too high to get reliable data, thus the DMSO concentration in the final solutions was lowered. To analyze whether a dilution of the MI in H<sub>2</sub>O and successive coupling leads to comparable yields of MI-modified proteases, we performed an enzyme activity assay as described in the main manuscript, with unmodified DENV2 NS2B/NS3 proteases in comparison with the proteases incubated 10 min at room temperature in presence of

10  $\mu$ M MI diluted with DMSO and H<sub>2</sub>O, respectively. In both cases, the same residual activities were seen, indicating no influence of the solvent on the modification reaction (**Figure SI4**).

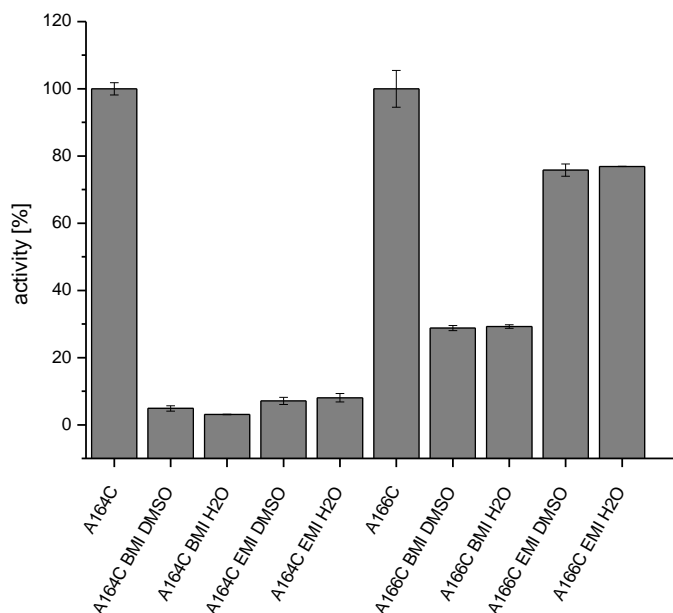


**Figure SI4:** Enzyme activity assay of the DENV2 A164C and the A166C mutants modified with either 10  $\mu$ M of the water- or DMSO-diluted MIs. Error bars show the standard deviations of the duplicate measurements.

CD spectra measured for the uncoupled and MI-coupled proteases are shown in **Figure SI5A** for A164C and **Figure SI5B** for A166C, respectively. No shift in secondary structures caused by modification with maleimide could be observed, pointing at an inactivation of the proteases just because of the MI-modification, while retaining the overall folding.



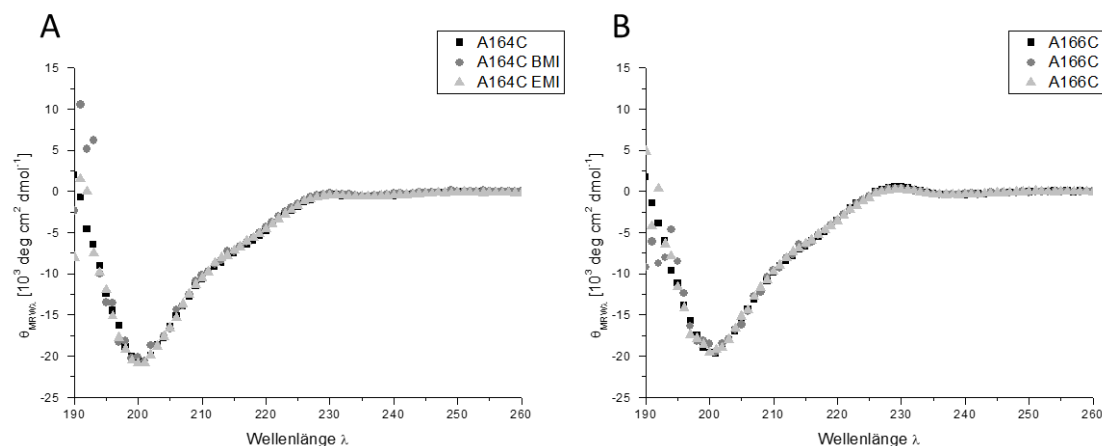


**Figure SI5:** Overlay of CD spectra as a comparison of maleimide-modified and unmodified DENV2 NS2B/NS3 protease. **A** represents the spectra of the A164C mutant, **B** shows the spectra of A166C, respectively.

As a result of the lack of  $\alpha$ -helical structures of the DENV2 NS2B/NS3 protease (

**Figure SI11**), at a first sight, the spectra look like those of random coiled structures. Therefore, further analyzes using the Beta Structure Selection method (BeStSel) online tool particularly suitable for  $\beta$ -rich structures were performed (**Table SI2**).<sup>3</sup>

**Table SI2:** Estimated secondary structures [%] of the unmodified and MI-modified DENV2 NS2B/NS3 protease cysteine mutants using the BeStSel online tool for analyzing the spectral data ranging from 200 to 250 nm.

Estimated secondary structure content (%)	A164C	A164C BMI	A164C EMI	A166C	A166C BMI	A166C EMI
Helix1 (regular)	0.40	0.00	0.70	0.00	0.00	0.00
Helix2 (distorted)	0.00	0.00	0.00	0.00	0.00	0.00
Anti1 (left-twisted)	0.00	0.00	0.00	0.00	0.00	0.00

Anti2 (relaxed)	2.40	0.90	2.40	3.40	3.90	3.80
Anti3 (right-twisted)	23.00	23.20	22.80	22.60	20.80	22.40
Parallel	0.00	0.00	0.00	0.00	0.00	0.00
Turn	13.20	13.90	13.60	13.30	13.40	13.80
Others	61.00	62.00	60.50	60.60	61.90	60.00
Helix	0.40	0.00	0.70	0.00	0.00	0.00
Antiparallel	25.40	24.20	25.30	26.10	24.60	26.20
Parallel	0.00	0.00	0.00	0.00	0.00	0.00
Turn	13.20	13.90	13.60	13.30	13.40	13.80
Others	61.00	62.00	60.50	60.60	61.90	60.00
Spectral deviation						
RMSD	0.0606	0.0928	0.0650	0.0907	0.1005	0.0852
NRMSD	0.0097	0.0148	0.0104	0.0147	0.0167	0.0142

## 5 DOCKING STUDIES

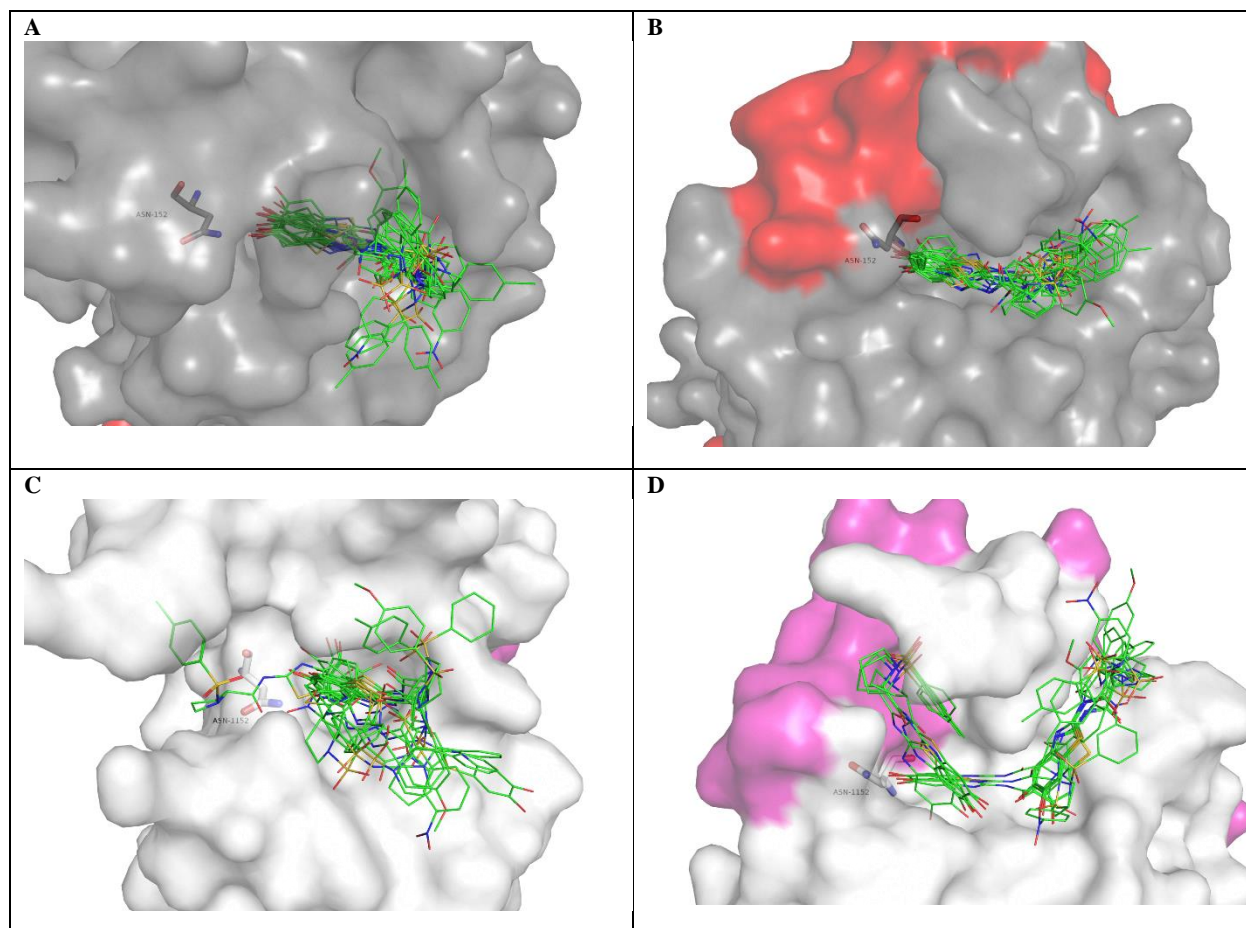


**Figure SI6.** Superposition of predicted binding modes of compounds **6a/b**, **7a/b**, **8a/b**, **10a**, **11a/b**, **12a/b**, **14a/b**, **35** (as lines with green carbon atoms) in complex with A) DENV protease open conformation (PDB code 2FOM). B) DENV protease closed conformation (PDB code 3U1I). C) ZIKV protease open conformation (PDB code 5GXJ) and D) ZIKV protease closed conformation (PDB code 5LC0). Asn152 (DENV protease) and Asn1152 (ZIKV protease), respectively, are represented as sticks for orientation. DENV NS3 is illustrated as grey surface, NS2B as red surface; ZIKV NS3 as white surface, NS2B as magenta surface.

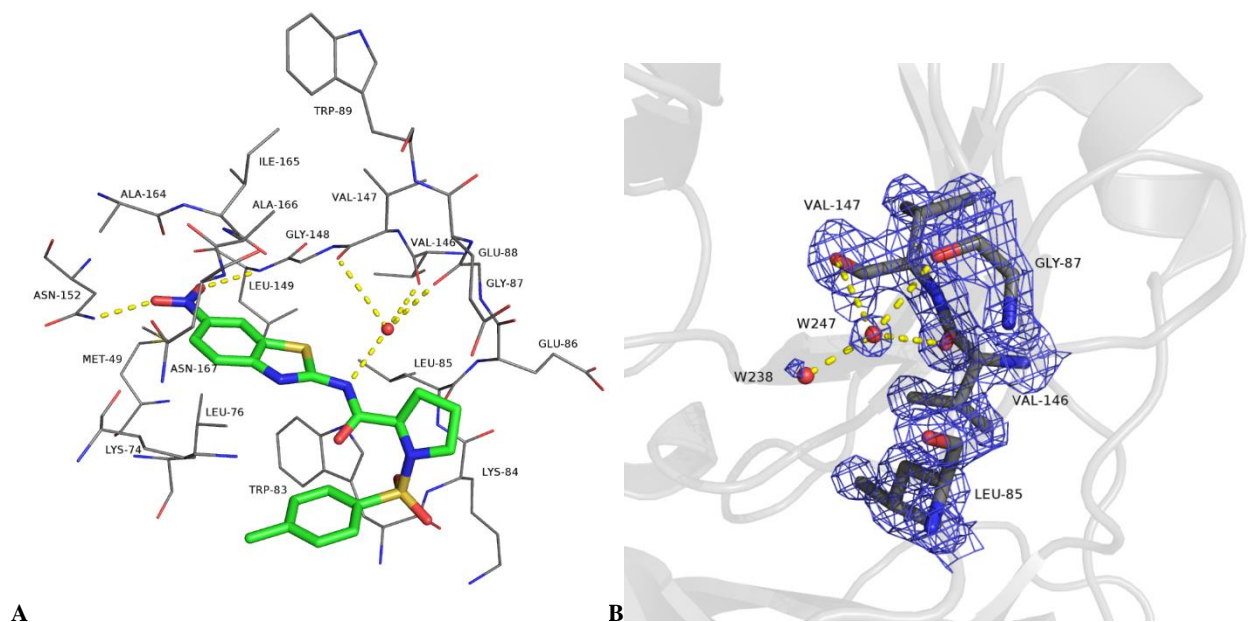


**Figure SI7.** A) Predicted binding mode of the 6-nitro-benzothiazole compound **22** (green carbon atoms) in complex with the open conformation of DENV protease (grey carbon atoms, PDB code 2FOM). Electrostatic interactions are illustrated as yellow dashes. B) 2Fo-Fc electron density map (PDB code 2FOM) of water molecule W247 and surrounding residues are contoured at  $1.5 \sigma$ . Possible H-bonds of W247 are illustrated as yellow dashes. W238 with lower electron density is supposed to be less stable bound and displaced by the amide NH-moiety of the ligand.

**Table SI3:** Rank and FlexX-scores of all 62 compounds within the binder and non-binder discrimination test set for ROC analysis. Compounds **Wu 1** – **SI19** were taken from Wu et al. 2015.<sup>4</sup> Docking was performed against DENV protease *open* (PDB code 2FOM), *closed* (PDB code 3U1I) and ZIKV protease *open* (PDB code 5GXJ) and *closed* (PDB code 5LC0) conformation using LeadIT-2.3.2.

Compound	Binder / Non-binder	Receptor							
		2FOM		3U1I		5GXJ		5LC0	
		Rank	Score	Rank	Score	Rank	Score	Rank	Score
<b>6b</b>	binder	16	-28.08	18	-22.69	8	-21.47	7	-21.81
<b>7b</b>	binder	13	-28.28	29	-20.48	23	-19.9	25	-18.84
<b>12b</b>	binder	20	-27.55	4	-24.25	40	-18.43	18	-19.55
<b>6a</b>	binder	6	-30.04	2	-25.21	18	-20.51	10	-20.89
<b>21a</b>	binder	4	-32.05	26	-20.99	11	-21.11	12	-20.75
<b>35</b>	binder	8	-28.93	1	-25.44	9	-21.36	2	-24.32
<b>7a</b>	binder	28	-26.81	20	-22.01	47	-18.13	37	-17.56
<b>12a</b>	binder	9	-28.39	9	-23.1	21	-20.17	41	-16.78
<b>17b</b>	non-binder	59	-18.32	51	-16.28	48	-18.05	58	-13.69
<b>17a</b>	non-binder	62	-17.81	61	-12.71	50	-17.93	52	-14.57
<b>9</b>	binder	30	-26.71	10	-23.04	42	-18.24	26	-18.62
<b>18b</b>	non-binder	43	-23.84	28	-20.62	6	-22.7	42	-16.4
<b>18a</b>	non-binder	21	-27.54	39	-18.99	29	-19.44	31	-17.99
<b>10a</b>	binder	31	-26.44	12	-22.93	43	-18.24	21	-19.3
<b>15a</b>	binder	15	-28.1	8	-23.42	2	-24.44	5	-22.28
<b>11a</b>	binder	37	-25.37	31	-20.18	37	-18.9	44	-16.22
<b>10b</b>	binder	34	-26.26	16	-22.82	38	-18.74	38	-17.5
<b>15b</b>	binder	26	-26.98	27	-20.96	3	-24.31	6	-22.18
<b>8a</b>	binder	10	-28.38	23	-21.41	10	-21.2	14	-20.3
<b>8b</b>	binder	42	-24.34	19	-22.16	32	-19.1	17	-19.75
<b>20</b>	non-binder	60	-18.14	53	-15.98	51	-17.92	49	-14.99
<b>19b</b>	non-binder	61	-17.84	50	-16.29	58	-16.64	62	-12.73
<b>19a</b>	non-binder	58	-19.65	62	-12.44	52	-17.78	63	-12.68
<b>14b</b>	binder	1	-34.89	5	-24.09	5	-22.8	23	-19.23
<b>14a</b>	binder	12	-28.36	6	-23.78	15	-20.9	3	-22.86

<b>13a</b>	binder	24	-27.09	13	-22.88	41	-18.37	9	-21.29
<b>11b</b>	binder	38	-25.36	30	-20.36	19	-20.38	34	-17.78
<b>13b</b>	binder	11	-28.37	3	-24.72	17	-20.69	32	-17.98
<b>22</b>	binder	17	-27.95	25	-21.11	49	-18.01	16	-19.85
<b>30a</b>	binder	35	-25.65	36	-19.27	28	-19.44	29	-18.22
<b>30b</b>	binder	41	-24.35	42	-18.2	24	-19.77	22	-19.29
<b>31</b>	binder	52	-22.14	11	-22.95	54	-17.32	45	-15.8
<b>21b</b>	binder	32	-26.36	38	-19.14	33	-19.07	1	-24.91
<b>26 (R config.)</b>	binder	27	-26.91	14	-22.84	30	-19.4	35	-17.58
<b>32</b>	binder	48	-22.89	32	-20.16	20	-20.34	4	-22.54
<b>26 (S config.)</b>	binder	19	-27.93	7	-23.6	13	-21.05	30	-18.03
<b>33</b>	non-binder	33	-26.36	46	-17.16	14	-20.99	15	-20.28
Wu 1	binder	36	-25.47	40	-18.98	35	-19.02	33	-17.83
Wu 2	binder	2	-32.47	52	-16.11	7	-22.56	40	-17.12
Wu 3	binder	14	-28.24	57	-14.82	53	-17.71	48	-15.41
Wu 4	binder	3	-32.07	45	-17.51	31	-19.20	19	-19.49
Wu 5	binder	18	-27.93	17	-22.71	27	-19.50	8	-21.3
Wu 6 (1)	binder	25	-27.05	15	-22.83	1	-24.49	20	-19.47
Wu 7	non-binder	55	-20.7	59	-14.34	59	-16.29	56	-14.19
Wu 8	binder	39	-24.62	35	-19.5	12	-21.06	28	-18.31
Wu SI1	non-binder	49	-22.78	60	-13.98	55	-17.12	50	-14.63
Wu SI2	binder	40	-24.58	44	-17.58	46	-18.14	51	-14.61
Wu SI3	non-binder	47	-23.14	55	-15.49	34	-19.06	46	-15.75
Wu SI4	binder	57	-19.98	54	-15.56	44	-18.22	53	-14.49
Wu SI5	binder	45	-23.68	58	-14.73	61	-15.98	59	-13.49
Wu SI6	binder	29	-26.71	24	-21.39	4	-23.68	11	-20.8

Wu SI7	non-binder	46	-23.54	22	-21.6	16	-20.82	24	-19.01
Wu SI8	non-binder	56	-20.68	37	-19.21	56	-17.08	36	-17.56
Wu SI9	binder	7	-29.23	21	-21.88	26	-19.68	27	-18.47
Wu SI10	non-binder	54	-20.71	47	-17.09	62	-15.04	54	-14.33
Wu SI11	non-binder	50	-22.56	49	-16.32	60	-16.09	55	-14.27
Wu SI12	binder	5	-30.25	41	-18.4	22	-19.95	39	-17.22
Wu SI13	binder	23	-27.41	48	-16.85	57	-16.86	61	-12.83
Wu SI14	non-binder	63	-16.06	63	-10.6	63	-13.56	57	-13.86
Wu SI15	non-binder	51	-22.41	56	-14.85	45	-18.18	60	-13.48
Wu SI16	binder	44	-23.82	33	-20.1	36	-18.99	47	-15.67
Wu SI17	binder	53	-21.46	34	-19.58	25	-19.73	43	-16.38
Wu SI18	binder	22	-27.5	43	-17.63	39	-18.52	13	-20.35

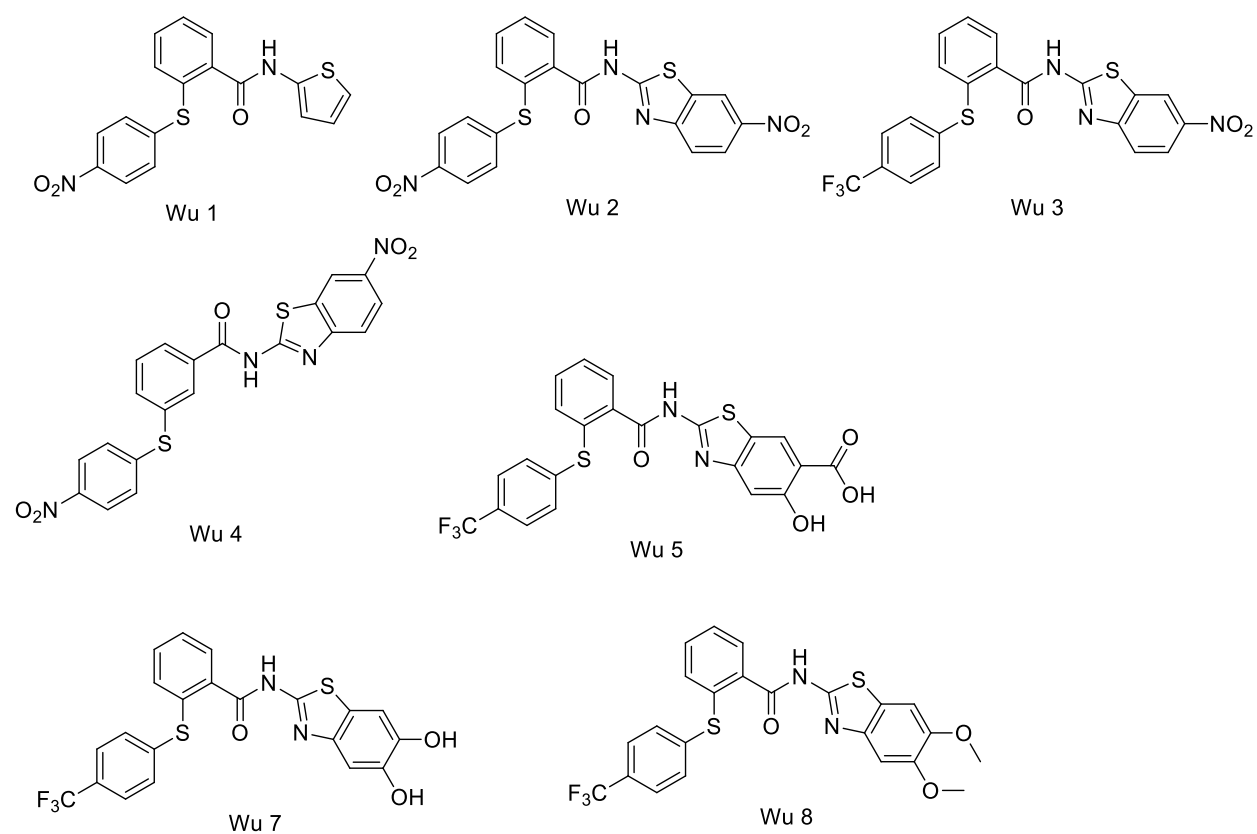


**Figure SI8.** Structures of Wu 1 – Wu 8.<sup>4</sup>

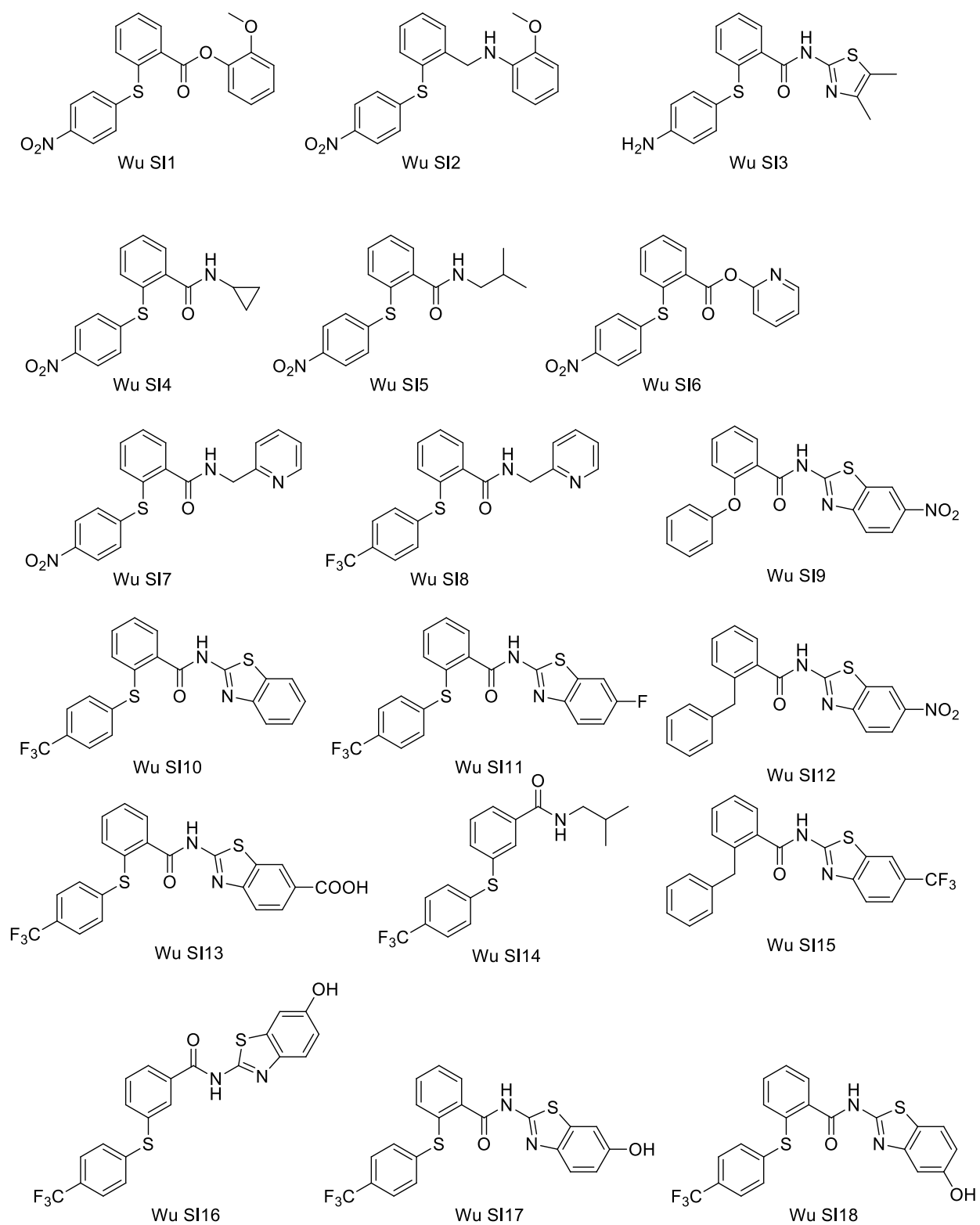


**Figure SI 9.** Structures of Wu SI1 – SI18.<sup>4</sup>



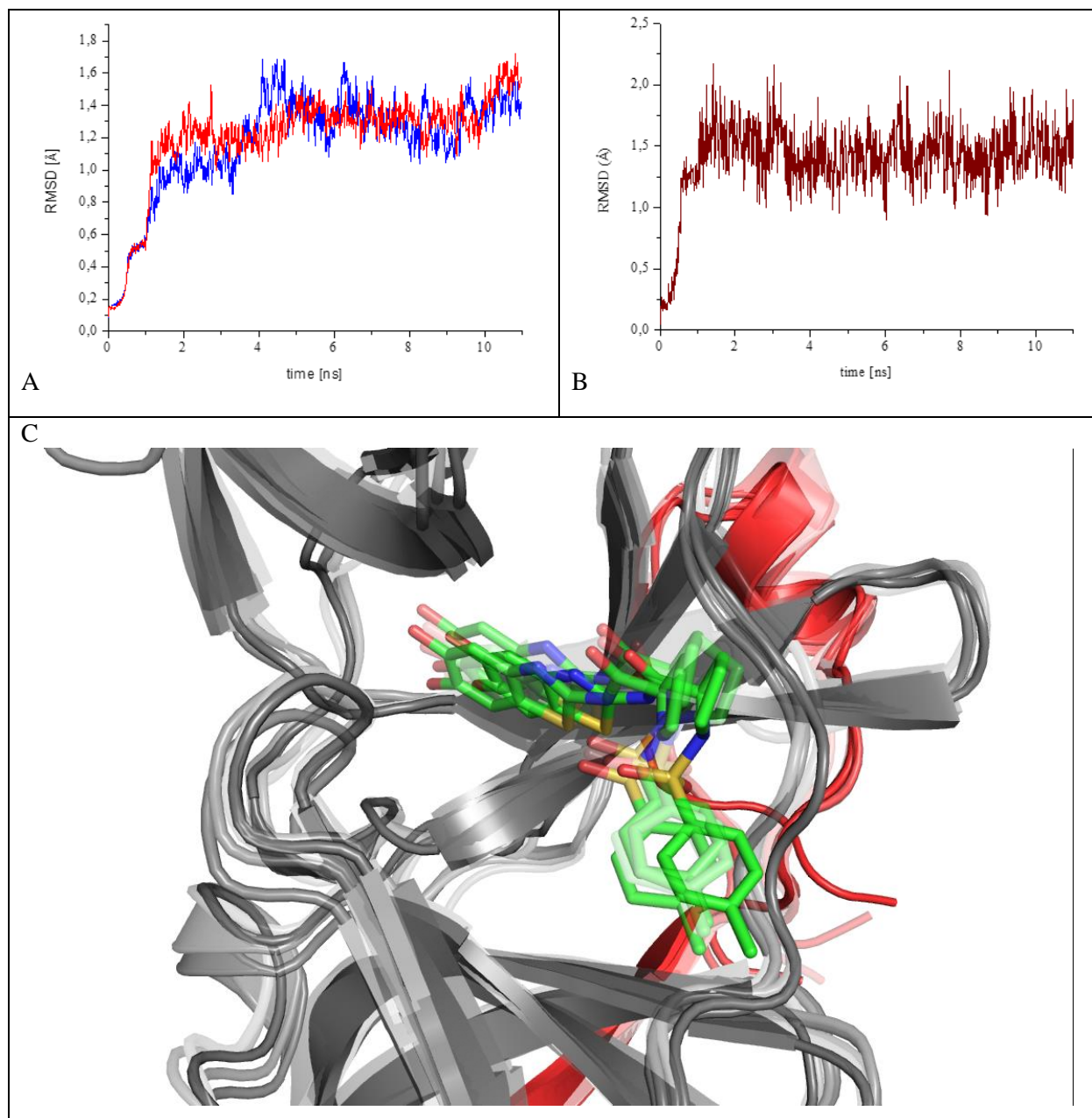


**Figure SI10.** A) Backbone RMSD-plot of DENV NS3/NS2B apo structure (blue line) and in complex with compound **7a** (red line) over 1 ns equilibration and 10 ns production run. B) **7a** non-hydrogen-atom RMSD-plot in complex with DENV NS2B/NS3 over 1 ns equilibration and 10 ns production run (average RMSD of 1.46 Å compared to starting structure generated by docking).

C) Superposition of trajectory snapshots after 2, 4, 6, 8 and 10 ns (with decreasing transparency) of the production run of DENGV NS2B/NS3-**7a** complex.

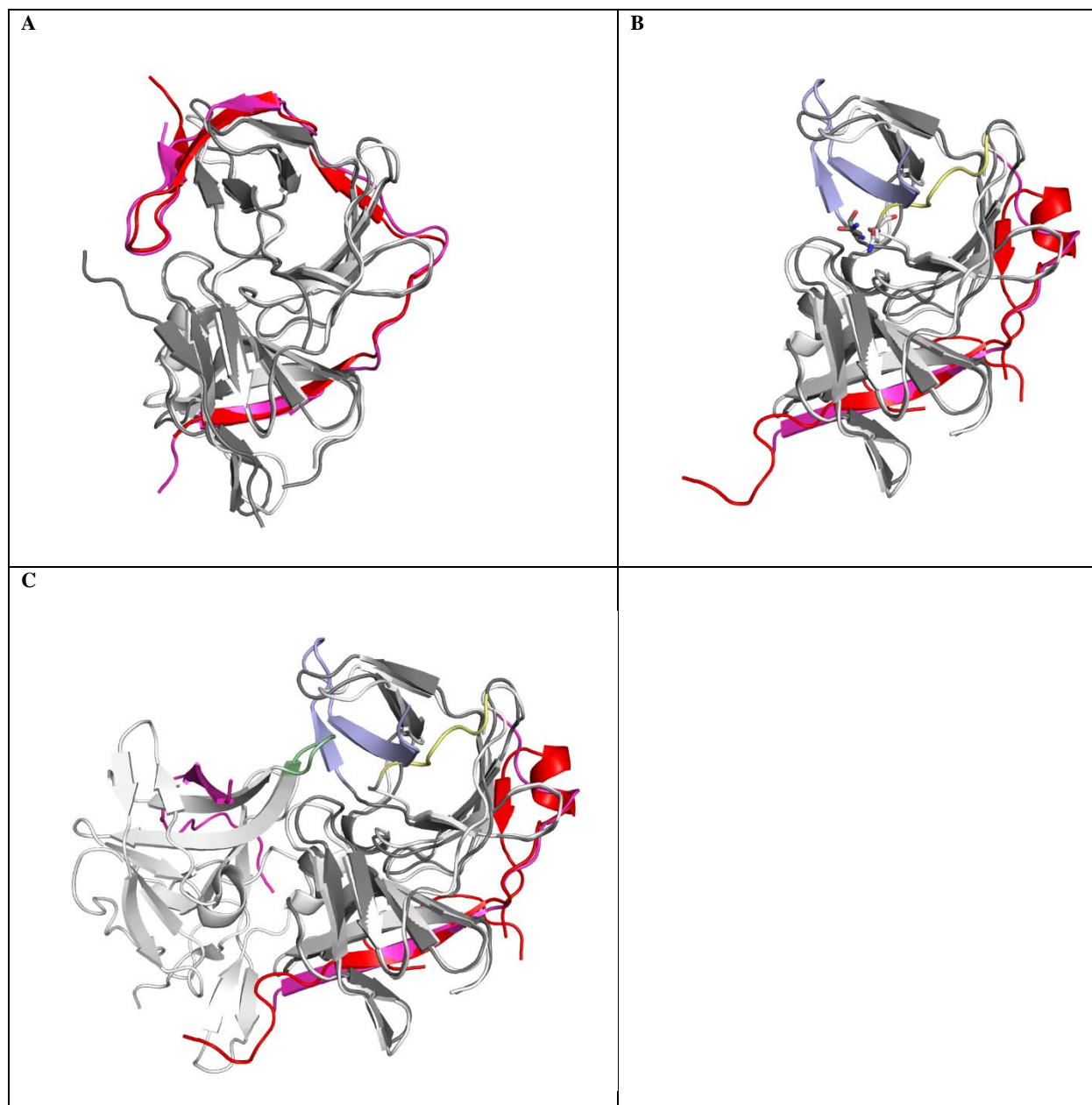
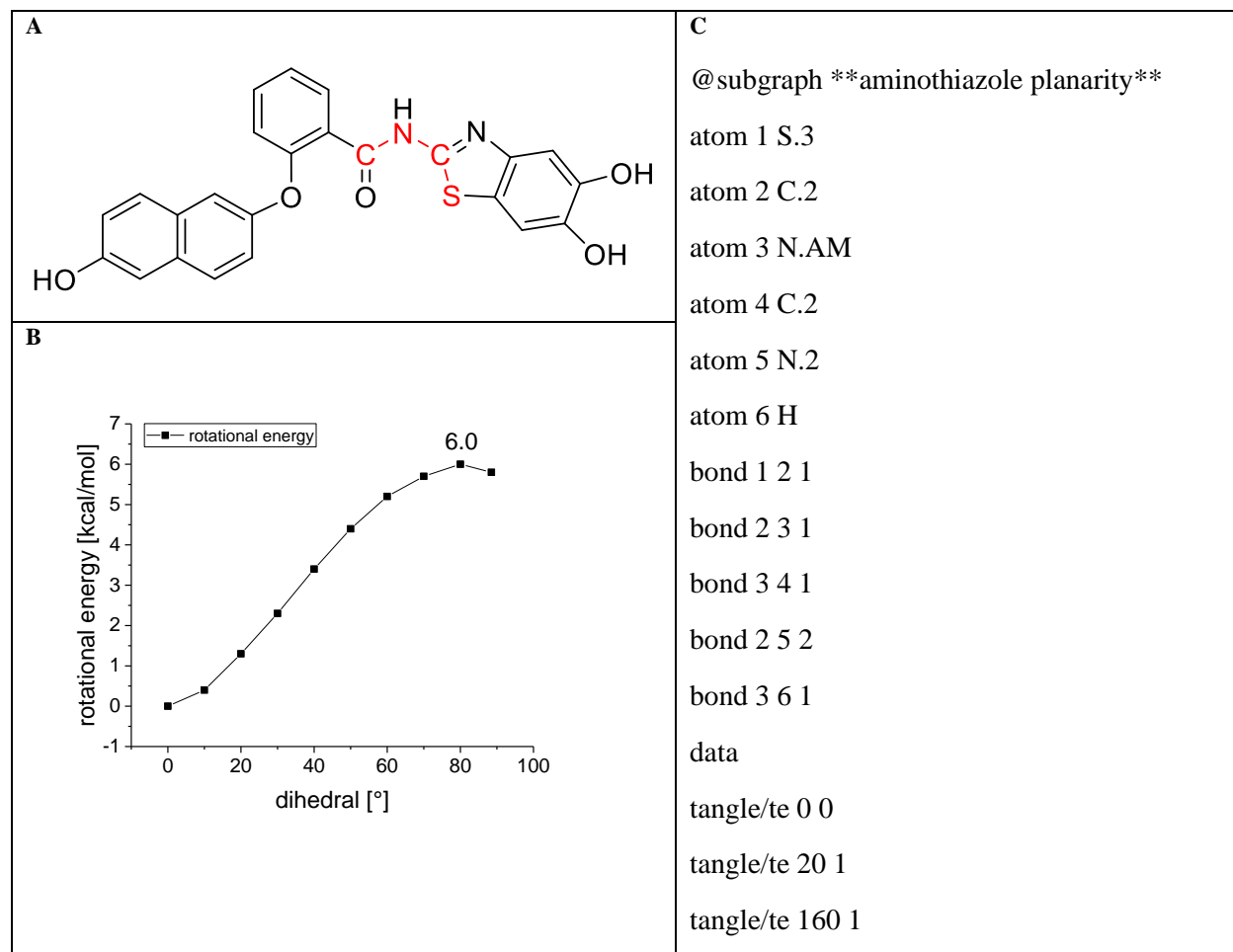


**Figure SI11.** A) Superposition of DENV (PDB code 3U1I) and ZIKV (PDB code 5LC0) NS2B/NS3 protease in the closed conformation ( $C_{\alpha}$  RMSD = 0.61 Å). DENV NS3 in grey. NS2B in red; ZIKV NS3 in white and NS2B in magenta; the color scheme also accounts for B and C. B) Superposition of DENV and ZIKV protease in open conformation (PDB codes 2FOM and 5GXJ, respectively;  $C_{\alpha}$  RMSD = 0.78 Å). Asn(1)152 is shown as sticks; subsequent residues differing in orientation are shown in light blue for the DENV protease and light yellow for the ZIKV protease. C) Additionally to B, the second monomer of the asymmetric unit from the ZIKV NS2B/NS3 is illustrated. Residues 1029-1032 preventing an open conformation analogue to DENV NS2B/NS3 by clashing are shown in light green.



	tangle/te 180 0 period 360 symmetry 180 <i>end</i>
--	---

**Figure SI12.** A) Structure of compound **1** with atoms for relaxed dihedral scan marked in red. B) Relaxed dihedral scan on B3LYP-D3/TZVP/PCM (solvent = water) level for red marked atoms. C) Torsion parameters to allow only dihedral angels 20° out of plane for marked atoms within FlexX docking.

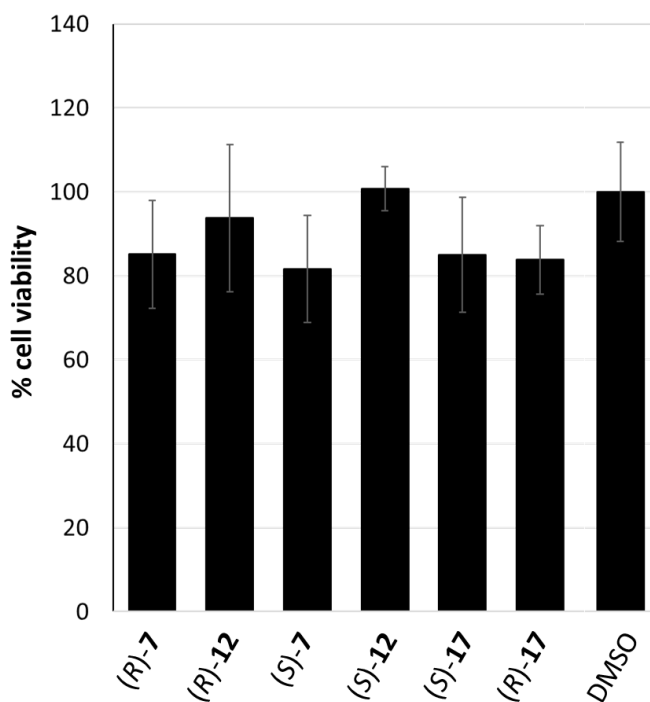
## 7 ANTIVIRAL ACTIVITY

**PLAQUE ASSAY ZIKV** The titer of cell culture supernatants was quantified by plaque assays. Vero cells were seeded in a 6-well plate in a concentration of  $3 \times 10^5$  cells/well and infected 6 h later with cell culture supernatant in a serial dilution in DMEM. The cells were washed once with PBS and covered with 37 °C pre-warmed DMEM containing 0.4% agarose 2 h p.i. After 15 min at room temperature, the plates were incubated for 96 h at 37 °C. To visualize the plaques, the agarose was removed gently, the cells were fixed for 20 min at room temperature with 4% formaldehyde in PBS and then stained for 15 min with 0.1% crystal violet in 20% ethanol. After the cells were washed once with water the titer (PFU/mL) was determined by counting the plaques in the well with the respective dilution.

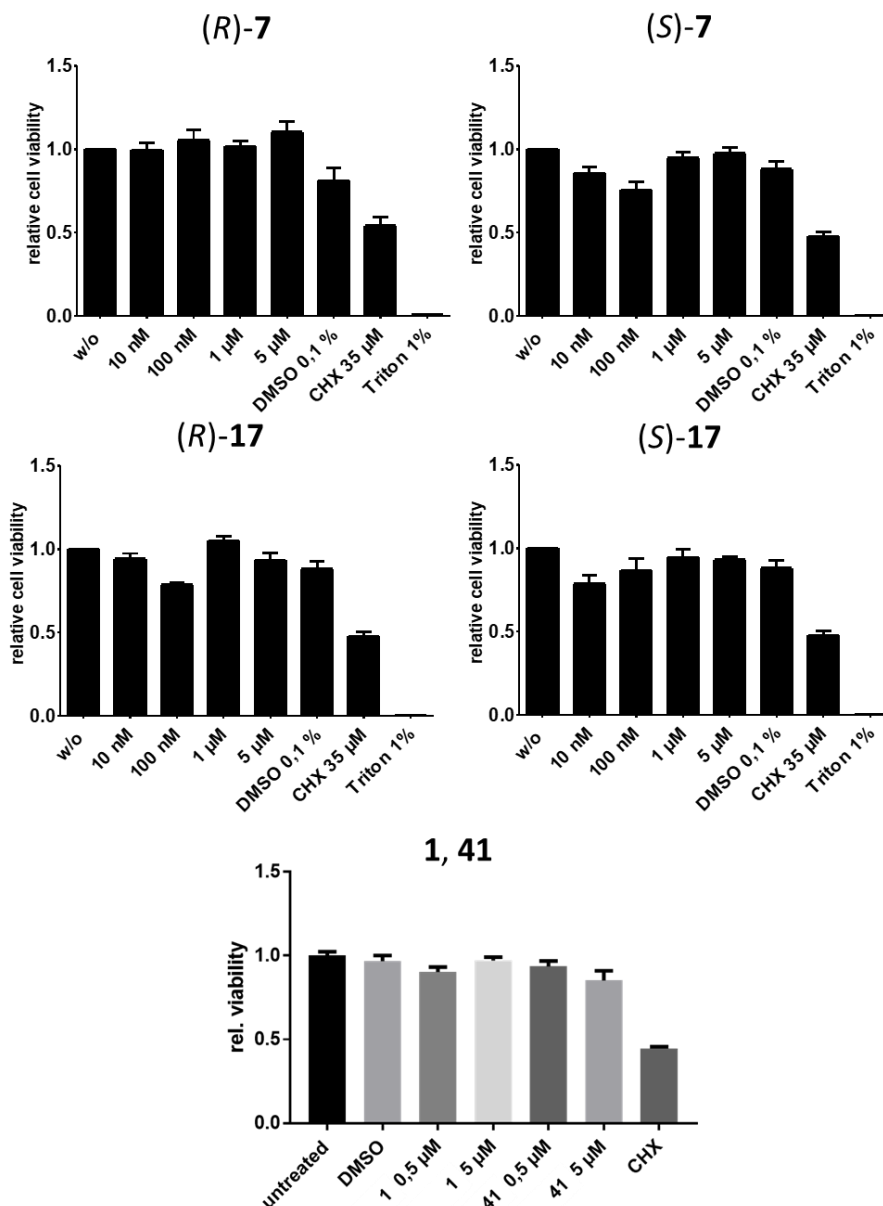
**IMMUNOFLUORESCENCE MICROSCOPY ZIKV** The experiments were performed in tissue culture plates harbouring cover slides. The A549 cells were then fixed with 4% formaldehyde in PBS for 20 min and then permeabilized with 0.5% Triton X-100 in PBS for 15 min at room temperature. After blocking with 1% BSA in PBS for 15 min at room temperature, the cells were stained with the antibody Anti-Flavivirus Group Antigen Antibody, clone D1-4G2-4-15 (Merck millipore, Darmstadt, Germany) in the dilution 1:200 and afterwards with the secondary antibody anti-mouse-AlexaFluor488 (Thermo Fisher Scientific) and DAPI for 1 h at room temperature in a humid chamber. After both antibody incubations, the coverslips were washed three times with PBS at room temperature. Finally, the cells were mounted with Mowiol on microscope slides. Immunofluorescence staining was analyzed using a confocal laser scanning microscope (CLSM 510 Meta) with Zen 2009 Software (both from Carl Zeiss, Oberkochen, Germany). The same software was used to calculate the corrected total cell fluorescence (CTCF).

STATISTICAL ANALYSIS ZIKV Results are presented as means  $\pm$  standard errors of the means (SEMs) from at least three independent experiments. The significance of the results was analyzed by unpaired two-tailed Student's *t*-test, using GraphPad Prism, version 6.07 for Windows (GraphPad Software, San Diego, CA, USA). In all figures the statistical significance is compared to the control group. Statistical significance is represented in figures as follows:

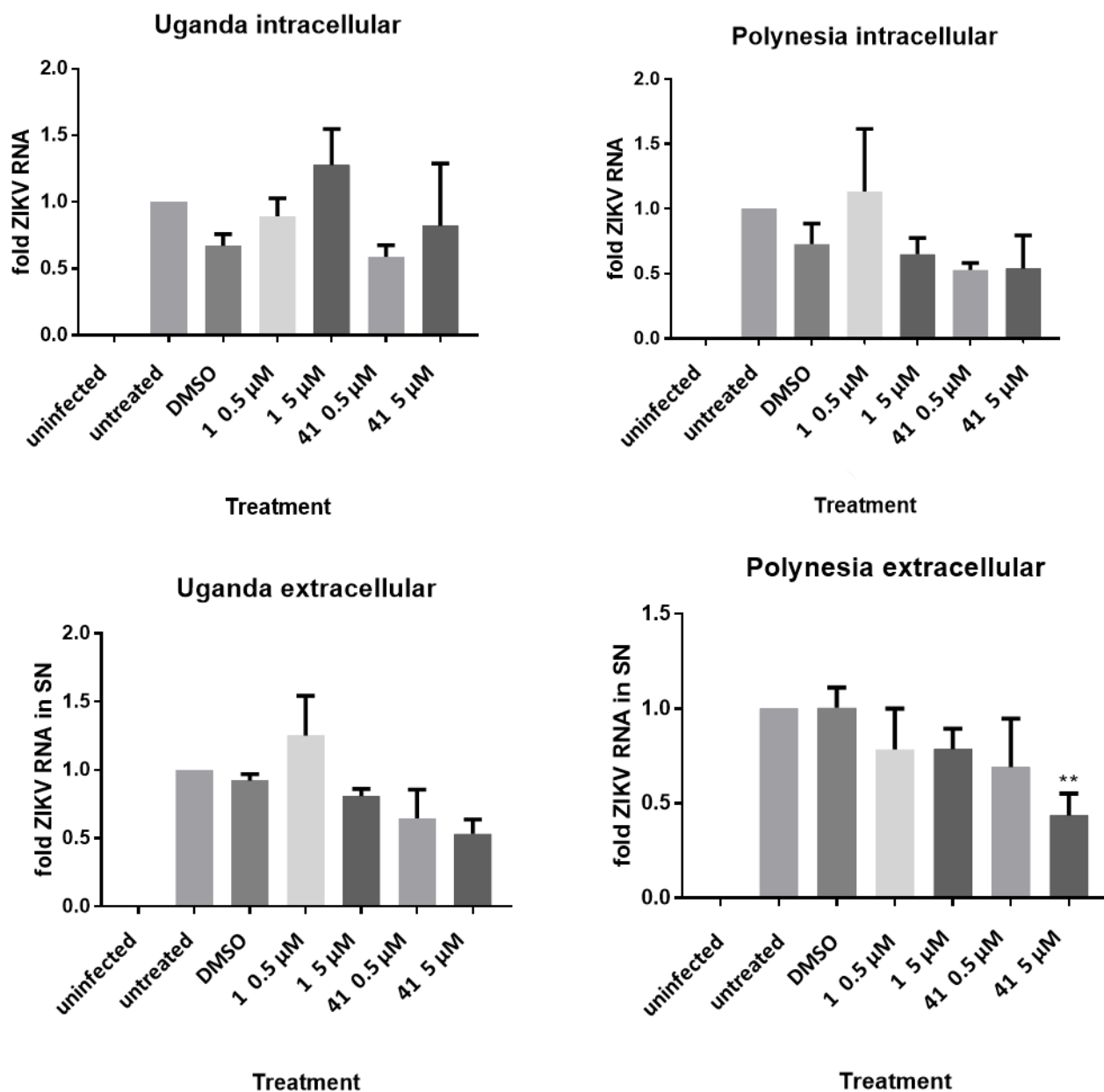
ns = not significant =  $p > 0.05$ ; \* =  $p \leq 0.05$ ; \*\* =  $p \leq 0.01$ ; \*\*\* =  $p \leq 0.001$ ; \*\*\*\* =  $p \leq 0.0001$ .



**Figure SI 13.** Cell toxicity tests of (R)-7, (S)-7, (R)-12, (S)-12, (R)-17 and (S)-17 on Vero cells. Cell cytotoxicity of the compounds at 10  $\mu$ M after 4 days of incubation was determined by a cell proliferation assay with DMSO as a control.

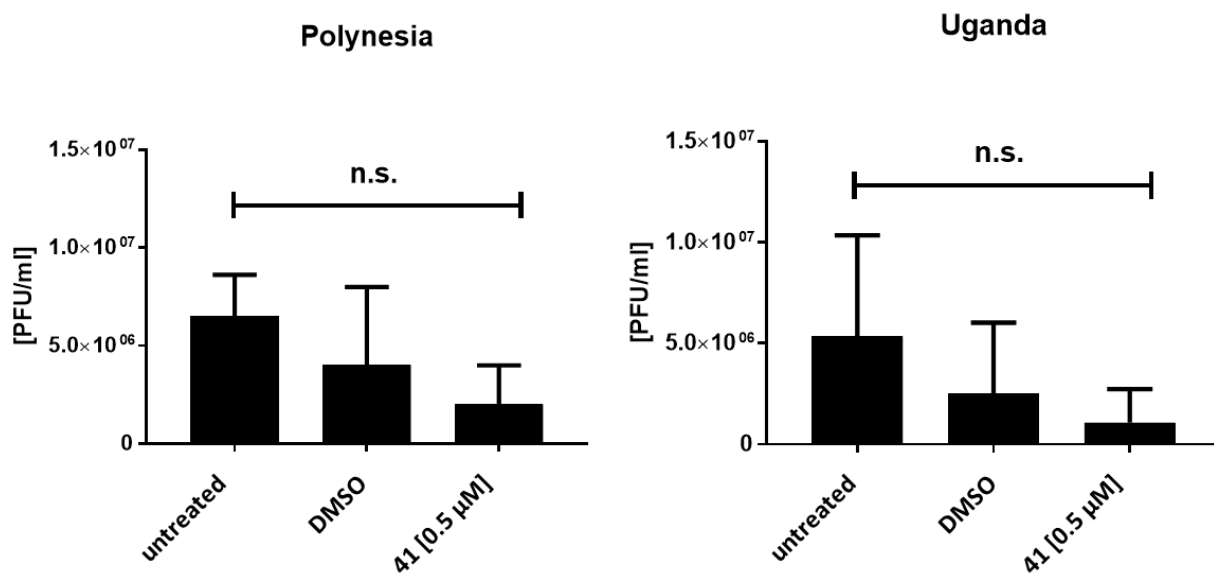


**Figure SI 14.** Cell toxicity tests of (R)-7, (S)-7, (R)-17, (S)-17, **1** and **41** on A549 cells. Cell cytotoxicity of the compounds at the indicated concentrations was determined by the PrestoBlue Cell viability reagent after 24 h. Cycloheximide (CHX) was used as a positive control at a concentration of 70  $\mu\text{M}$ .

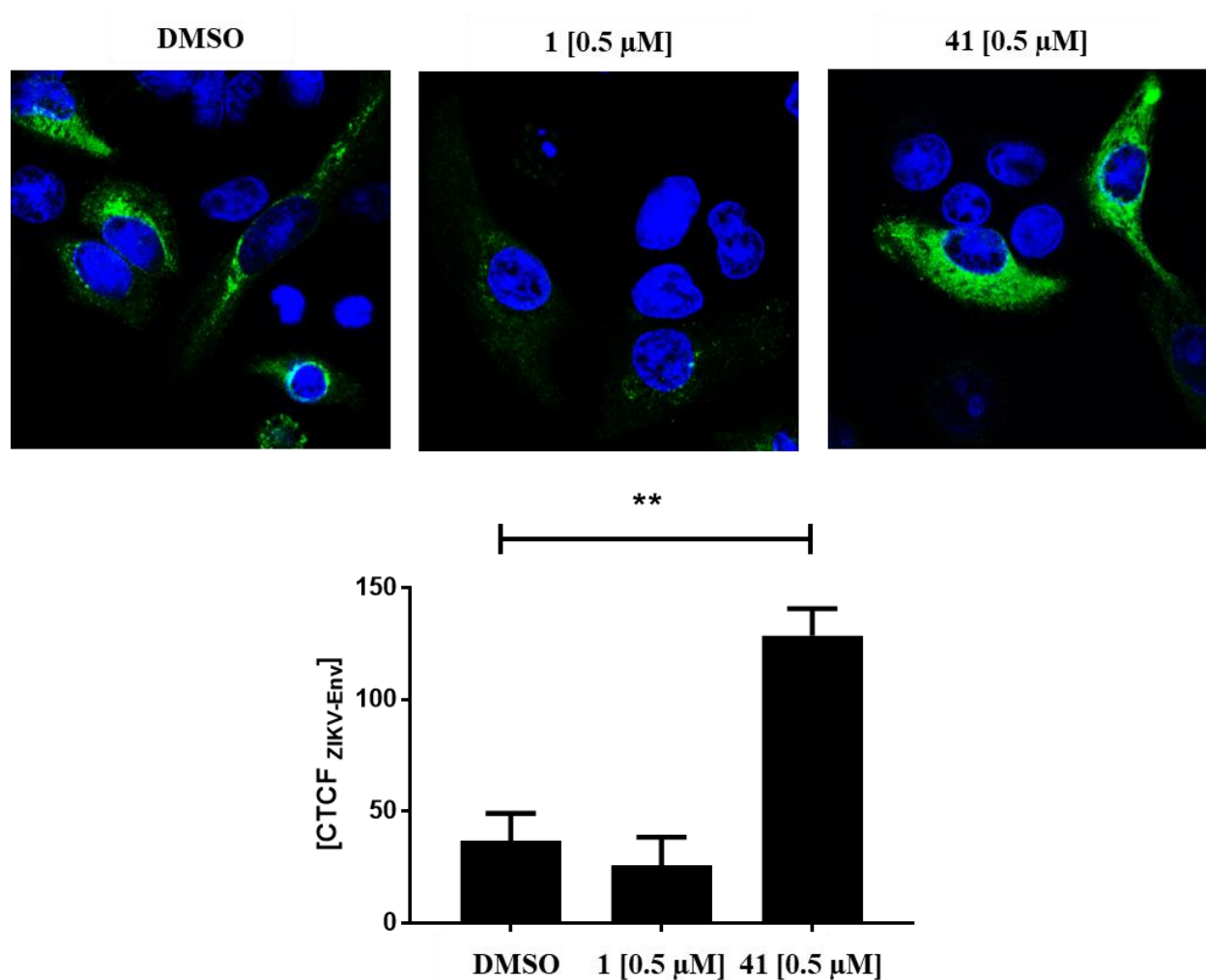


**Figure SI15.** Effect of the treatment of ZIKV Uganda or French Polynesia Strain infected cells with **1** and **41**. A549 cells were infected with ZIKV virus and the compounds were added at different concentrations. Viral RNAs were isolated, quantified by RTqPCR and normalized to the untreated control.

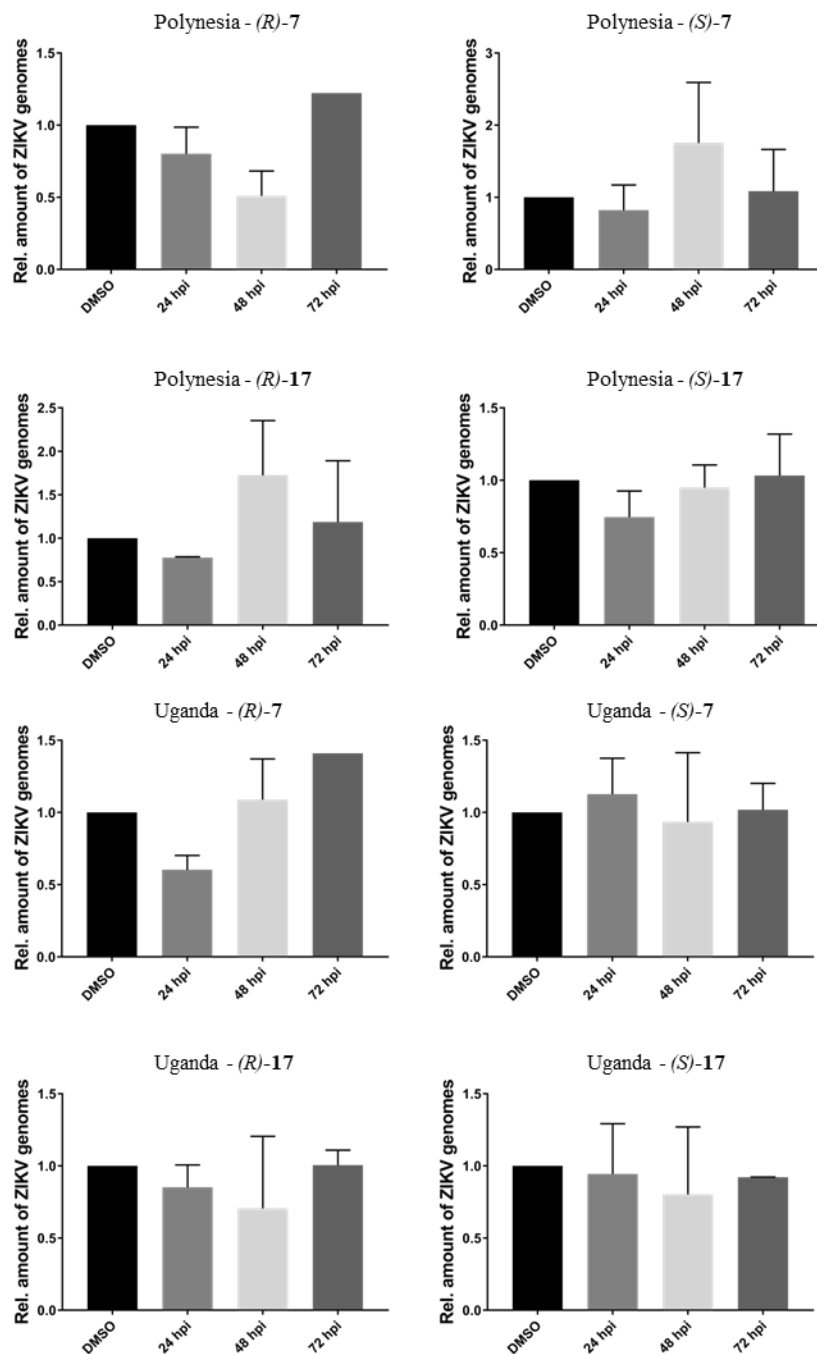




**Figure SI16.** Effect of **41** on the inhibition of the French Polynesia or Uganda ZIKV strain. Vero cells were seeded, infected with ZIKV cell culture supernatant and covered with agarose. After incubating for 96 h, the cells were fixed with formaldehyde, stained with crystal violet and the titer as plaque forming units (PFU) was determined by counting.

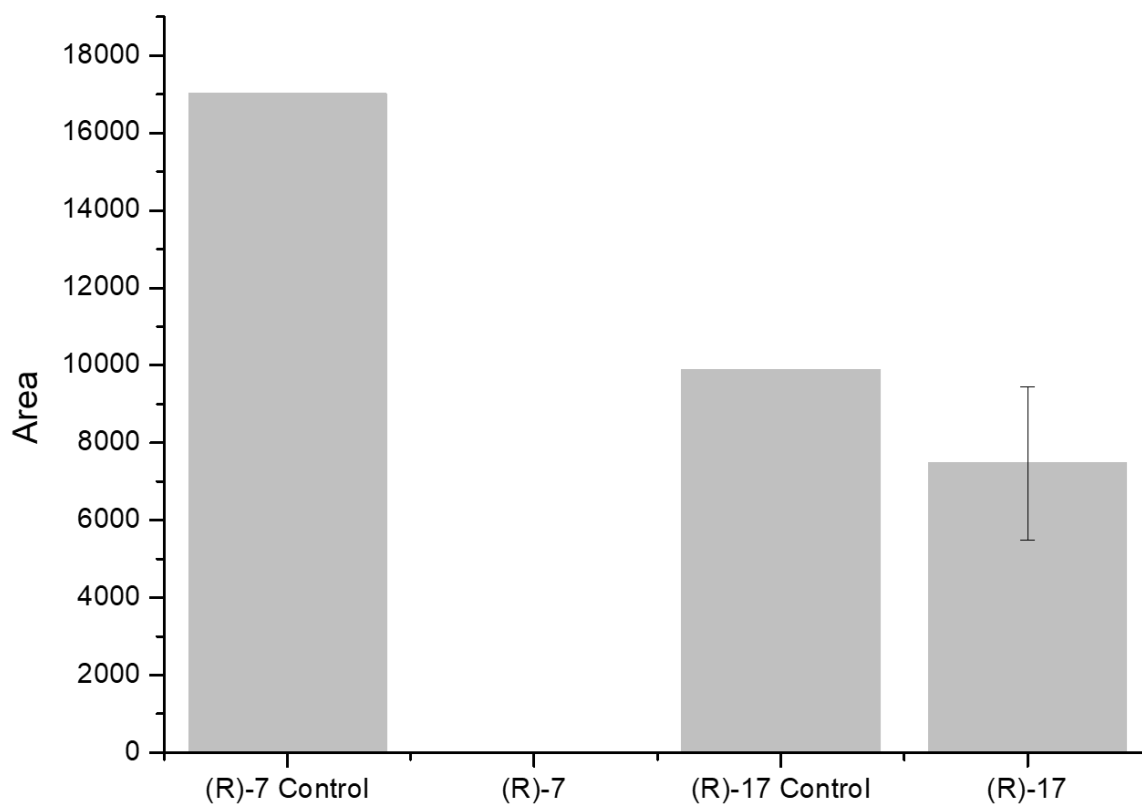


**Figure SI17.** **41** leads to a redistribution of ZIKV Env protein (green) from the ER to the cytoplasm. A549 Cells were infected with ZIKV and treated with **1** and **41**. After fixing and permeabilizing, the cells were stained with an anti-flavivirus antigen antibody and a secondary antibody, inspection by confocal scanning microscopy was done and the corrected total cell fluorescence (CTCF) was determined. DNA was stained with 4',6-diamidin-2-phenylindol (blue).



**Figure SI18.** Effect of the treatment of ZIKV Uganda or French Polynesia Strain infected cells with (R)-7, (S)-7, (R)-17, and (S)-17 at a concentration of 5  $\mu$ M. A549 cells were infected with ZIKV virus and the compounds were added at 5  $\mu$ M. Viral RNAs were isolated, quantified by RTqPCR and normalized to the untreated control.

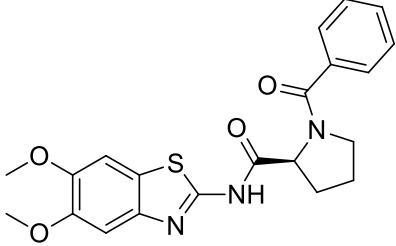
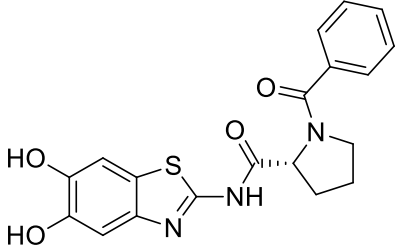
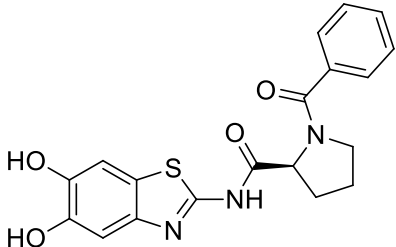
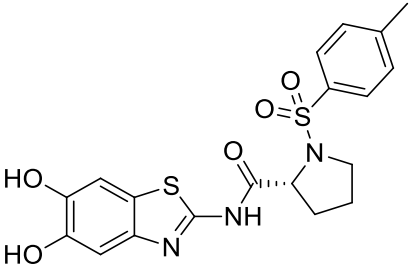
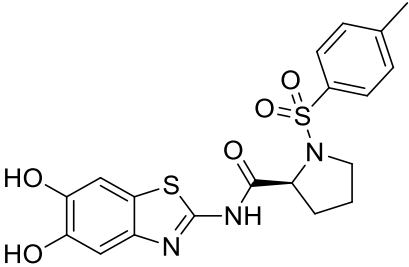
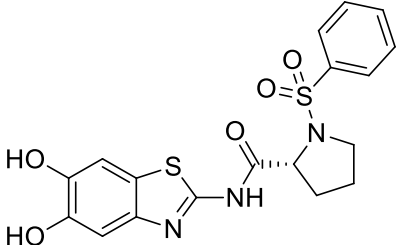
## 8 CELL PERMEABILITY

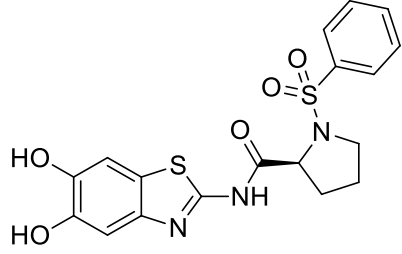
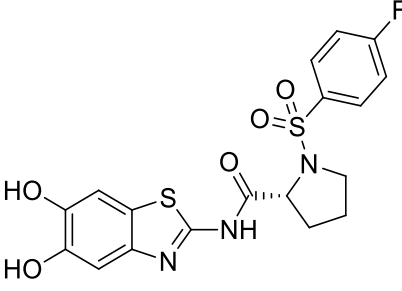
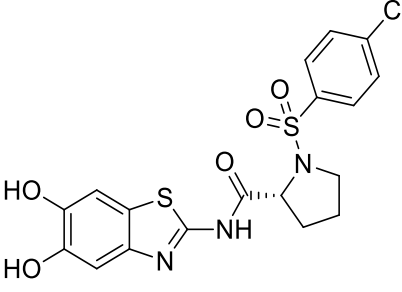
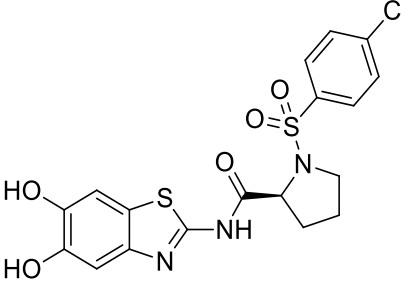
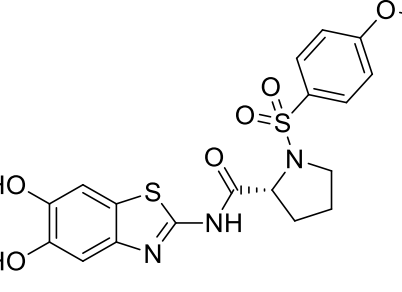


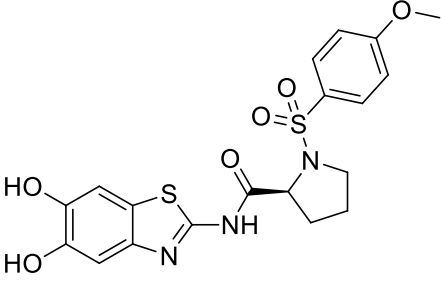
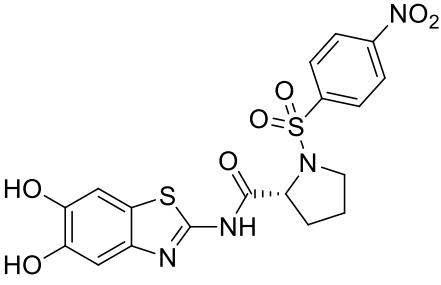
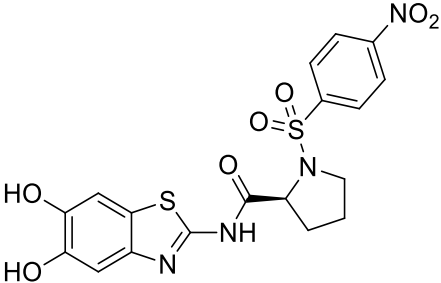
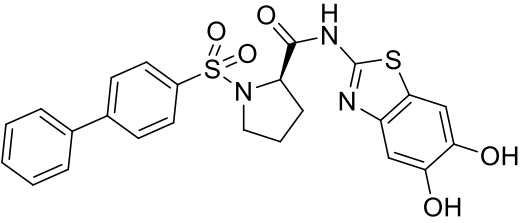
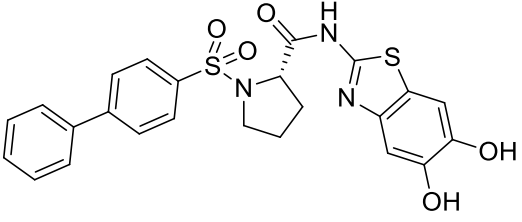
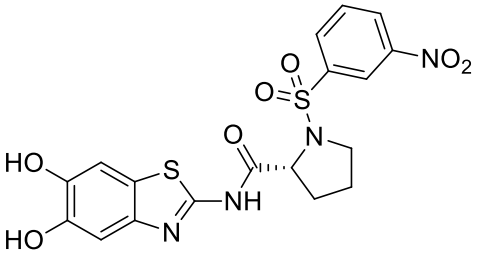
**Figure SI19.** MS areas from cell-permeability studies. A layer of Caco-2 cells was incubated with 10  $\mu$ M (*R*)-**7** and (*R*)-**17** for 3 hours and the donor and acceptor solutions were analyzed by LC-MS. Shown are the areas of the MS signals of the acceptor solution.

## 9 OVERVIEW OF ALL MANUSCRIPT COMPOUNDS WITH NUMBERS

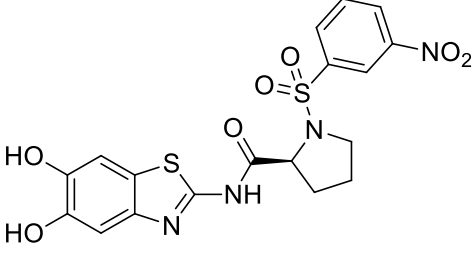
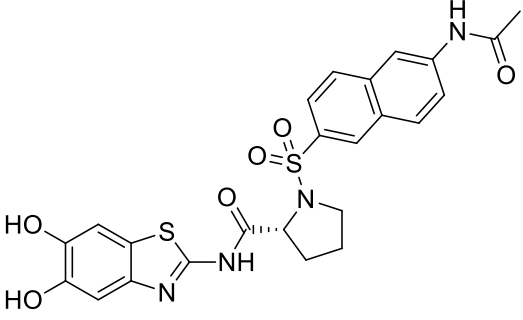
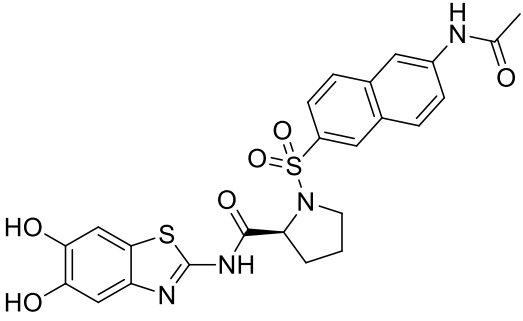
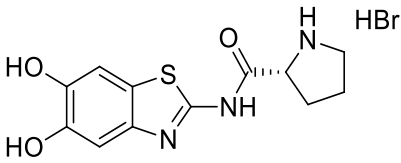
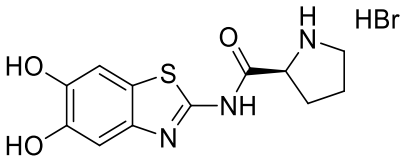
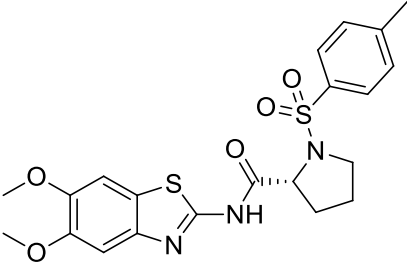
Compound	Structure
<b>1</b>	
<b>2</b>	
<b>(R)-3</b>	
<b>(S)-3</b>	
<b>(R)-4</b>	
<b>(S)-4</b>	
<b>(R)-5</b>	

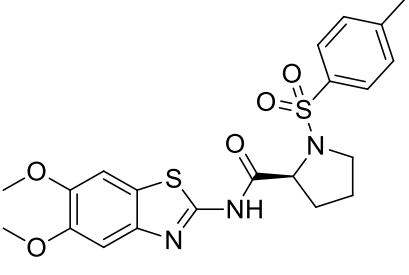
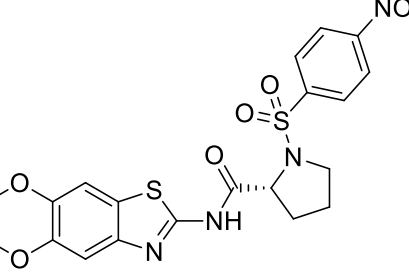
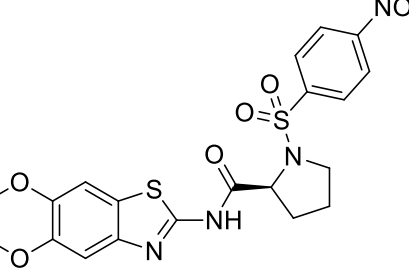
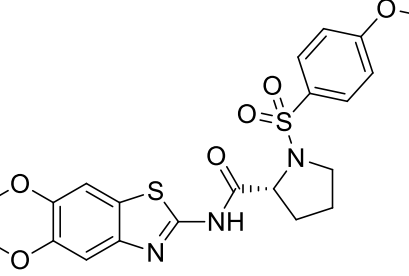
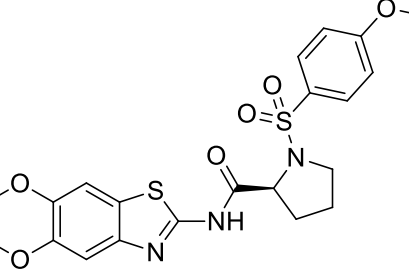
(S)-5	
(R)-6	
(S)-6	
(R)-7	
(S)-7	
(R)-8	

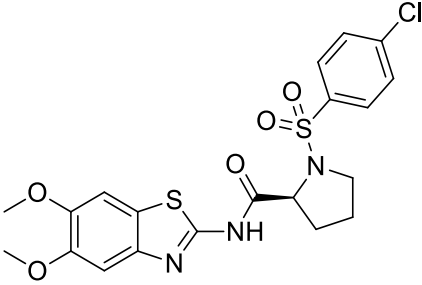
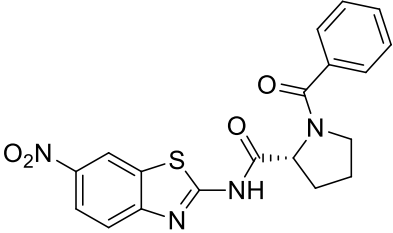
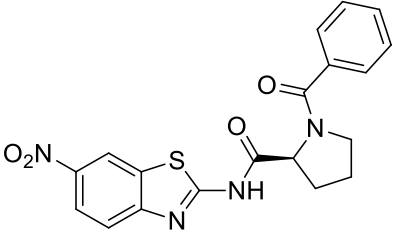
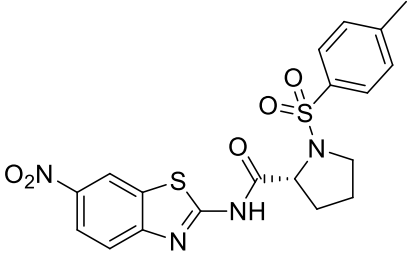
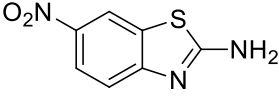
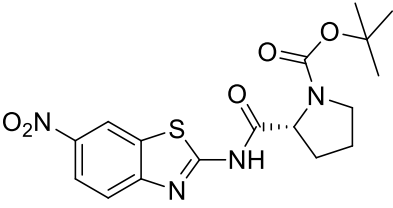
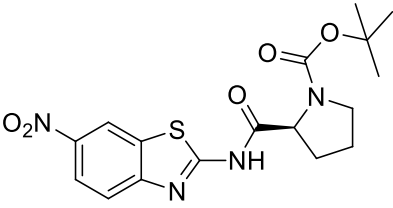
(S)-8	
9	
(R)-10	
(S)-10	
(R)-11	

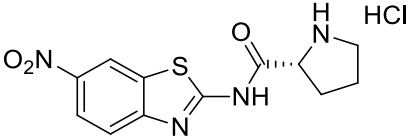
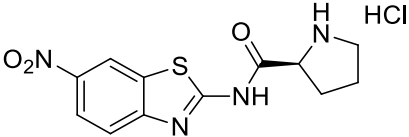
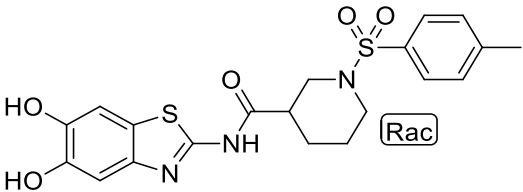
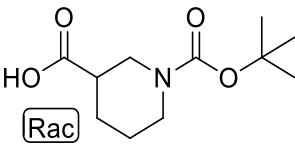
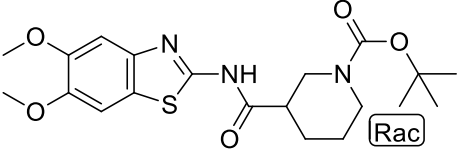
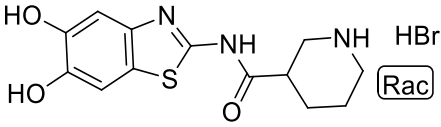
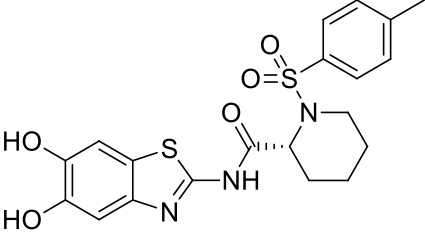
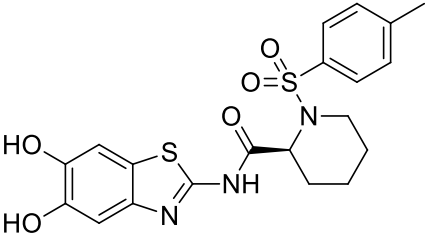
(S)-11	
(R)-12	
(S)-12	
(R)-13	
(S)-13	
(R)-14	

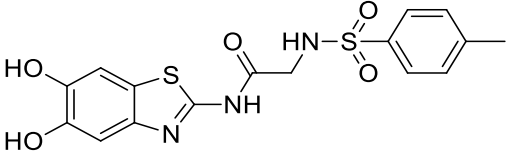
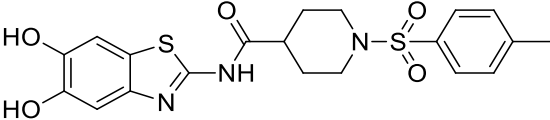
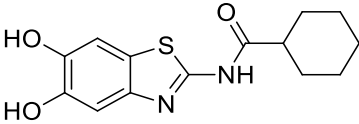
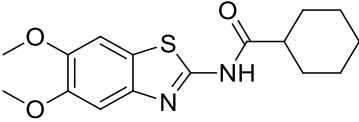
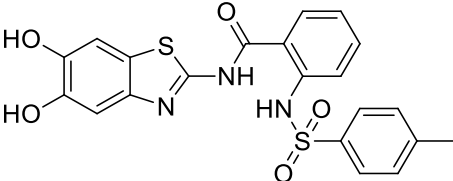
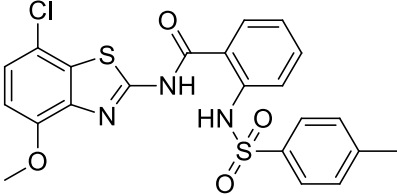
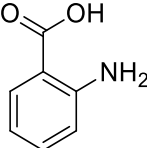
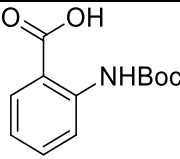
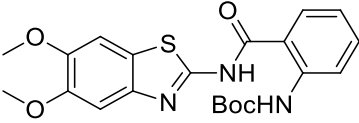


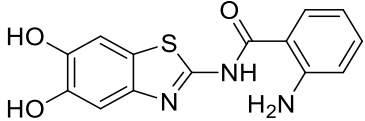
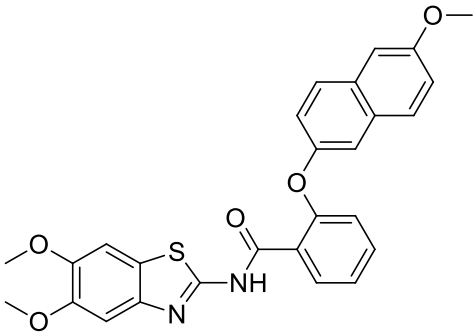
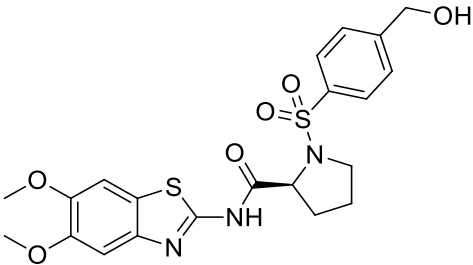
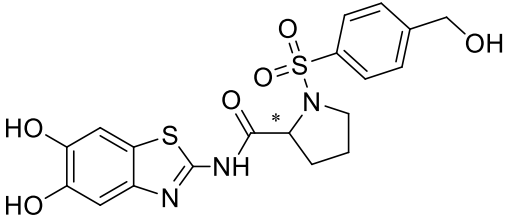
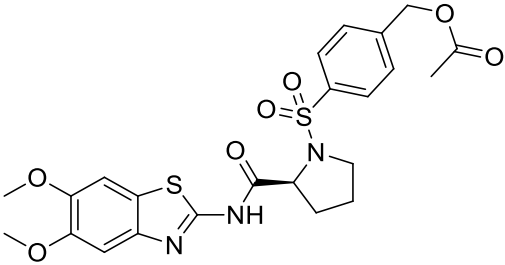
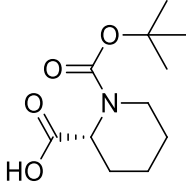
(S)-14	
(R)-15	
(S)-15	
(R)-16	
(S)-16	
(R)-17	

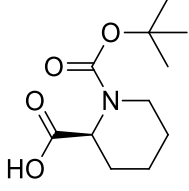
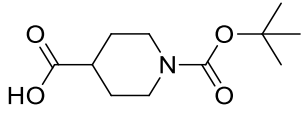
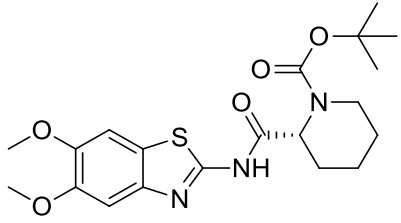
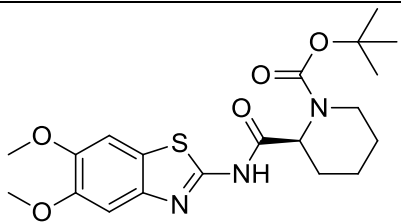
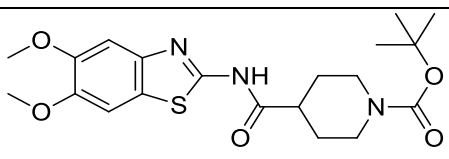
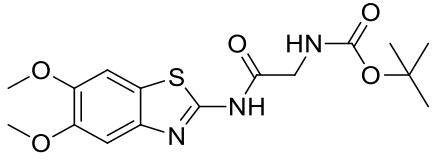
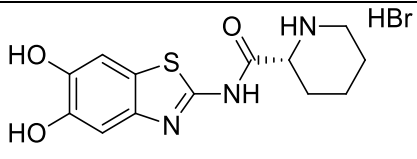
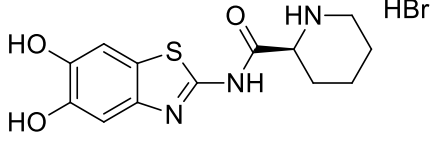
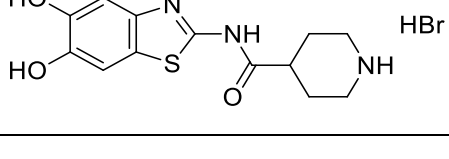
<b>(S)-17</b>	
<b>(R)-18</b>	
<b>(S)-18</b>	
<b>(R)-19</b>	
<b>(S)-19</b>	

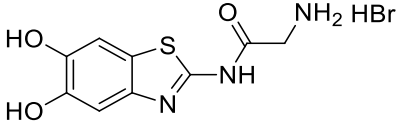
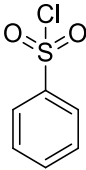
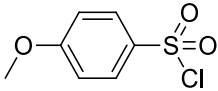
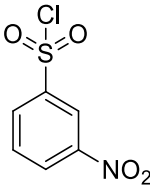
20	
(R)-21	
(S)-21	
22	
23	
(R)-24	
(S)-24	

<b>(R)-25</b>	
<b>(S)-25</b>	
<b>(RS)-26</b>	
<b>(RS)-27</b>	
<b>(RS)-28</b>	
<b>(RS)-29</b>	
<b>(R)-30</b>	
<b>(S)-30</b>	

31	
32	
33	
34	
35	
36	
37	
38	
39	

40	
41	
(S)-42	
43	
(S)-44	
(R)-45	

<b>(S)-45</b>	
<b>46</b>	
<b>(R)-47</b>	
<b>(S)-47</b>	
<b>48</b>	
<b>49</b>	
<b>(R)-50</b>	
<b>(S)-50</b>	
<b>51</b>	

52	
53	
54	
55	



## 10 REFERENCES

- (1) Wildman, S. A.; Crippen, G. M. Prediction of Physicochemical Parameters by Atomic Contributions. *J. Chem. Inf. Comput. Sci.* **1999**, *39*, 868–873.
- (2) Micsonai, A.; Wien, F.; Kernya, L.; Lee, Y.-H.; Goto, Y.; Réfrégiers, M.; Kardos, J. Accurate Secondary Structure Prediction and Fold Recognition for Circular Dichroism Spectroscopy. *Proc. Natl. Acad. Sci. U.S.A.* **2015**, *112*, E3095-103.
- (3) Greenfield, N. J. Using Circular Dichroism Spectra to Estimate Protein Secondary Structure. *Nat. Protoc.* **2006**, *1*, 2876–2890.
- (4) Wu, H.; Bock, S.; Snitko, M.; Berger, T.; Weidner, T.; Holloway, S.; Kanitz, M.; Diederich, W. E.; Steuber, H.; Walter, C.; Hofmann, D.; Weißbrich, B.; Spannaus, R.; Acosta, E. G.; Bartenschlager, R.; Engels, B.; Schirmeister, T.; Bodem, J. Novel Dengue Virus NS2B/NS3 Protease Inhibitors. *Antimicrob. Agents Chemother.* **2015**, *59*, 1100–1109.